and assuming a rupture velocity of 3 km s^{-1} and a depth of faulting of 15 km; this method is described by H. Kanamori *et al.* [*Geophys. Res. Lett.* **19**, 2267 (1992)].
25. L. K. Hutton *et al.*, *Calif. Geol.* **33**, 110 (1980).
26. R. Dokka and C. Travis, *Geophys. Res. Lett.* **17**, 1323 (1990).
27. Y. Bock *et al.*, *Nature* **361**, 337 (1993); G. Blewitt *et al.*, *ibid.*, p. 340.
28. Some examples are the 1932 *M* 7.4 Cedar Mountain, Nevada, the 1932 *M* 7.5 Chang Ma, China, the 1891 *M* 8 Nobi, Japan, the 1954 *M* 7.2 Fairview Peak–Dixie Valley, Nevada, and the 1957 Gobi-Altai, Mongolia, earthquakes.
29. This similarity is based on the assumption that the average depth to the base of the fault zone is the maximum depth of aftershocks, 15 km.
30 These events include the 1979 *M* 6.5 Imperial Valley, the 1984 *M* 6.2 Morgan Hill, the 1986 *M* 5.9 North Palm Springs, the 1987 *M* 6.6 Superstition Hills, and the 1989 *M* 6.9 Loma Prieta earthquakes.
31 However, the three well-known major San Andreas earthquakes (1857, 1906, and 1989) did not produce large off-fault aftershocks and had small aftershock sequences compared with those of other California events [low value of *a* in the equation in (*18*)]. Therefore, strong concerns about off-fault aftershocks may be unwarranted.
32. Slow-moving faults may have higher stress drops because they are more irregular and have had more time to strengthen between events [H. Kanamori and C. R. Allen, in *Earthquake Source Mechanics*, S. Das and C. H. Scholz, Eds. (American Geophysical Union, Washington, DC, 1986), vol. 6, pp. 566–574].
33. R. A. Harris and R. W. Simpson, *Nature* **360**, 251 (1992); S. C. Jaumé and L. R. Sykes, *Science* **258**, 1325 (1992).
34. The rate of earthquakes from 1945 to 1984 has been compared with that from 1985 to the summer of 1992. The rate of occurrence of $\geq M$ 4 earthquakes did not change, but the relative distribution of magnitudes changed significantly, with larger earthquakes more common in the later period. This difference implies an increase by a factor of 6, to 12% per year, in the probabilities of a *M* 7 earthquake in southern California.
35. D. C. Agnew and L. M. Jones, *J. Geophys. Res.* **96**, 11959 (1991).
36. L. M. Jones, *Eos* **73**, 357 (1992).
37. From Global Positioning System data collected at 13 sites by the U.S. Geological Survey, Southern California Earthquake Center, and the California Department of Transportation; processed by the U.S. Geological Survey and the Southern California Earthquake Center. The inversion was tested for slip on a four-segment geometry with varied location and was well-determined and stable for total moment results, yielding a range of 0.9×10^{27} to 1.1×10^{27} dyne-cm (K. Hudnut *et al.*, *ibid.*, p. 365.
38. The radiated energy estimated with TERRAscope by the method described by H. Kanamori and co-workers (*Bull. Seismol. Soc. Am.*, in press) is 4.3×10^{23} ergs, which corresponds to the energy radiated by a M_L 7.3 earthquake if M_L did not saturate. See also H. Kanamori and colleagues in (*24*).
39. We thank D. Agnew, A. Densmore, J. Dolan, K. Gross, D. Jackson, S. Larsen, M. Lisowski, M. Rymer, Z. Shen, and J. Svarc for helpful discussions and assistance. We also thank the seismic analysts of the Southern California Seismographic Network who have processed the Landers earthquake data, including R. Dollar, R. Geary, D. Given, W. Huston, S. Perry-Huston, R. Robb, and L. Wald. Data collection and processing partially supported by the Calfech Earthquake Research Affiliates Emergency Earthquake Fund and by the Southern California Earthquake Center (contribution number 25), which is funded by the National Science Foundation and the U.S. Geological Survey. Additional support from Division of Geological and Planetary Sciences, California Institute of Technology (contribution number 5217).

A Nickel Metal Hydride Battery for Electric Vehicles

S. R. Ovshinsky, M. A. Fetcenko, J. Ross

Widespread use of electric vehicles can have significant impact on urban air quality, national energy independence, and international balance of trade. An efficient battery is the key technological element to the development of practical electric vehicles. The science and technology of a nickel metal hydride battery, which stores hydrogen in the solid hydride phase and has high energy density, high power, long life, tolerance to abuse, a wide range of operating temperature, quick-charge capability, and totally sealed maintenance-free operation, is described. A broad range of multi-element metal hydride materials that use structural and compositional disorder on several scales of length has been engineered for use as the negative electrode in this battery. The battery operates at ambient temperature, is made of nontoxic materials, and is recyclable. Demonstration of the manufacturing technology has been achieved.

The interest in electrically powered vehicles extends nearly as far back as interest in vehicles powered by hydrocarbon fuels. Throughout this period, however, there has been a major technological barrier to the development of practical electric vehicles (EVs) that can compete in performance and cost with those that use internal combustion (IC) engines. This barrier has been the lack of an economical battery with sufficient energy density and other essential performance criteria. In this article, we describe the science and technology of a nickel metal hydride (NiMH) battery that will permit future EVs to replace IC-powered vehicles in many applications.

S. R. Ovshinsky and M. A. Fetcenko are at Energy Conversion Devices, Inc., 1675 West Maple Road, Troy, MI 48084. J. Ross is in the Chemistry Department, Stanford University, Palo Alto, CA 94305, and consultant to Energy Conversion Devices, Inc.

Recently, U.S. federal and state governments have been providing an impetus for the development of an EV industry through legislation aimed at increasing national energy independence and reducing the impact of automobile emissions on the environment. California has passed laws that demand that 2% of new cars sold in 1998 be emission-free, and this percentage is slated to grow to 10% by the year 2003; 12 eastern states are planning similar laws. A comprehensive energy bill passed by Congress contains a tax credit for EV buyers. This bill also requires state and federal governments to purchase alternative-fuel fleet vehicles, with the percentage of new, cleaner fuel vehicles growing to 90% by the year 2000. It is expected that EVs will make up an increasing portion of alternative fuel vehicles as the market grows.

There are several important advantages of EVs compared with IC-powered vehicles. First, EVs are emission-free: they produce no pollution during operation. This quality is particularly important in city centers where congested automobile traffic is the primary source of local air pollution. The overall unwanted emissions that result from combustion of fossil fuels for the generation of electricity are also far less per mile of EV travel than the emissions produced directly by a fossil fuel–powered car. This fact, discussed in detail in a study by the Electric Power Research Institute (EPRI) (*1*), results from the sophisticated emissions controls that can be used economically by large, efficient, central power-generation facilities. Second, the EPRI study also details how the primary energy efficiency of electric transportation can exceed the efficiency of gasoline-powered vehicles in many instances. For example, the study shows that electric-powered commercial fleet vans that are used in urban areas have a significant advantage in energy efficiency over their gasoline-powered counterparts, traveling about 1100 miles per barrel of oil consumed at the power plant compared with 620 miles per barrel of oil refined into gasoline. This difference results primarily from the higher energy efficiency of power plant combustion—approximately twice as high as combustion of gasoline in an IC engine in urban traffic. Third, conversion from cars directly powered by fossil fuel to ones powered by electricity can shift the choice of hydrocarbon fuels that are consumed in the United States from oil to coal and gas. This change could possibly reduce the oil imports and, consequently, reduce the U.S. trade imbalance and the strategic vulnerability of its energy supply. Photovoltaic and other renewable energy sources are

also increasingly available to generate pollution-free electricity for EVs.

In response to the need to develop a practical battery for EVs, the U.S. federal government authorized the establishment of the U.S. Advanced Battery Consortium (USABC) in 1990. Under the aegis of the Department of Energy, USABC brings together Chrysler, Ford, General Motors (GM), and EPRI to sponsor research and development of EV batteries. Although energy density is one of the most important requirements for an EV battery system, USABC has identified a number of other battery criteria as necessary for the development of economically viable EVs (Table 1 provides the primary midterm goals of USABC). Ovonic Battery Company (OBC), a subsidiary of Energy Conversion Devices, has received the first contract from USABC toward the continued development and fabrication of the company's proprietary NiMH batteries and has agreed to establish EV battery production facilities.

In this article, we describe the science and technology of the Ovonic NiMH battery, with emphasis on the materials science aspects of the metal hydride (MH) electrode and their effect on battery performance (2). The MH electrode offers an important opportunity for materials engineering and optimization when compared with negative electrodes for other nickel-based battery systems. In these other systems, the negative electrode (Cd, Zn, or Fe) is typically fabricated from relatively pure elemental metals, and the oxidation-reduction reactions associated with battery charge and discharge convert the electrode back and forth between a metal and a metal oxide that is a poor electric conductor. This type of chemical reaction can be undesirable in a practical battery design because of accompanying changes in the physical properties of the electrode. Changes in the mechanical integrity and surface morphology of the electrode as a result of dissolution and recrystallization and of its reduced electrical conductivity in the oxidized state are sources of many of the performance deficiencies in these systems.

The MH electrode, by contrast, uses a chemical reaction that reversibly incorporates hydrogen into a metal alloy. In this oxidation-reduction reaction both chemical states are metallic, and so electrical conductivity is high in both the charged and discharged states. Furthermore, the small size of the hydrogen atom allows it to enter the metal lattice during formation of the hydride (reduced) state with only about 10% volumetric expansion and without the changes in crystallography associated with oxidation and reduction of the Cd, Zn, or Fe electrodes.

In effect, the MH negative electrode can be regarded as a matrix for the chemical incorporation of the hydrogen atom. In the Ovonic NiMH battery, we have exploited the ability of this matrix to be engineered through the use of multi-element alloys, using compositional and structural disorder to produce materials with desirable battery properties.

Cell Reactions

The NiMH battery, which has a nominal voltage of 1.2 V, stores hydrogen as a reaction product in the solid hydride phase, unlike the nickel-hydrogen battery that stores hydrogen as a high-pressure gas. The negative electrode of a conventional NiMH battery consists of a hydrogen storage material (3–5) that can allow electrochemical storage and release of hydrogen during battery charge and discharge processes. The nickel hydroxide positive electrode (6–9) is electrochemically reversible between $Ni(OH)_2$ and nickel oxyhydroxide, usually written as NiOOH. At both electrodes, oxidation-reduction reactions take place in an alkaline medium consisting of 30% by weight KOH in water. During charge, the $Ni(OH)_2$ electrode is oxidized and the MH electrode is reduced. As a result, water is separated into hydrogen and hydroxyl ions, with hydrogen reacting with the metal in the negative electrode to form MH. At the positive electrode, the hydroxyl ion reacts with the $Ni(OH)_2$ electrode to form NiOOH. This reaction results in a change in the Ni oxidation state from +2 to +3. The half-cell reactions on charge and discharge of the battery can be written as

$$M + H_2O + e^- \underset{\text{Discharge}}{\overset{\text{Charge}}{\rightleftarrows}} MH + OH^- \quad (1)$$

$$Ni(OH)_2 + OH^- \underset{\text{Discharge}}{\overset{\text{Charge}}{\rightleftarrows}} NiOOH + H_2O + e^- \quad (2)$$

As a consequence of reactions 1 and 2, there is no net change in electrolyte quantity or concentration over the charge-discharge cycle. This result contrasts with other alkaline electrolyte systems such as NiCd where water is generated at both electrodes during charge and consumed at both electrodes during discharge. Although transient electrolyte concentration gradients can occur in the NiMH battery, its constant average concentration has the important consequences of good overall performance in gas recombination, kinetics, high- and low-temperature operation, and resistance to cycle-life limitations produced by corrosion and swelling.

Material Requirements

The MH materials used for an NiMH battery electrode must satisfy an extensive list of requirements. Above all, the amount of hydrogen that the MH material can absorb determines the electrochemical storage capacity of the electrode and, consequently, the energy storage capacity of the battery. It is desirable to have high electrode storage capacity that is electrochemically reversible. To ensure reversibility, an important aspect of the MH design is the range of metal-to-hydrogen bond strengths, which must be about 6 to 12 kcal mol^{-1}. If the bond strength is too weak, hydrogen will not react with the alloys and will be evolved as a gas. If the bond strength is too large, the MH electrode is extensively oxidized and does not store hydrogen reversibly.

Even with an optimally adjusted metal-hydrogen bond strength, the problem of electrode oxidation in the MH battery

Table 1. Primary USABC midterm performance goals for the EV battery and actual performance of the current OBC NiMH battery. DOD, depth of discharge.

Property	USABC	OBC
Specific energy (Wh kg^{-1})	80 (100 desired)	80*
Energy density (Wh per liter)	135	215*
Power density (W per liter)	250	470
Specific power (W kg^{-1}) (80% DOD in 30 s)	150 (>200 desired)	175
Cycle life (cycles) (80% DOD)	600	1000
Life (years)	5	10
Environmental operating temperature	−30° to 65°C	−30° to 60°C
Recharge time	<6 hours	15 min (60%) <1 hour (100%)
Self discharge	<15% in 48 hours	<10% in 48 hours
Ultimate projected price (dollars per kWh) (10,000 units at 40 kWh)	<$150	$200

*A specific energy of 80 Wh kg^{-1} and an energy density of 215 Wh per liter have been achieved in a laboratory prototype, with 50-Ah cells under a discharge rate at which the battery energy capacity is exhausted in 3 hours.

remains. The NiMH battery operates in a strongly oxidizing medium composed of a high-concentration alkaline electrolyte. Because many chemical elements react to form oxides in an alkaline electrolyte, it follows that if these elements are used as electrodes, they will oxidize and fail to store hydrogen reversibly. In addition, MH electrodes are typically designed for use in totally sealed batteries where oxygen recombination occurs at their surfaces. In this aggressively oxidizing environment, oxidation and corrosion resistance of MH electrode materials is critical. Because some oxidation at the metal-electrolyte interface is inevitable and because both passivation and corrosion can have adverse effects on battery performance, these unwanted processes must be controlled in a practical NiMH electrode design.

Another consideration in the use of hydride materials in NiMH batteries relates to electrochemical kinetics and transport processes. The power output of the battery depends critically on these processes. During discharge, hydrogen stored in the bulk metal must be brought to the electrode surface by diffusion. The hydrogen must then react with hydroxyl ions at the metal-electrolyte interface. As a consequence, surface properties such as oxide thickness, electrical conductivity, surface porosity and topology, surface area, and degree of catalytic activity affect the rate at which energy can be stored in and removed from the NiMH battery.

For the battery to operate as a sealed system, it must also tolerate the consequences of chemical reactions that occur during cell overcharge and overdischarge. In overcharge, oxygen gas is generated at the $Ni(OH)_2$-positive electrode and must recombine with hydrogen at the MH electrode to form water. In overdischarge, which occurs when a low-capacity cell in a series-connected string is subjected to reverse polarity, hydrogen is generated at the $Ni(OH)_2$ electrode and must be recombined at the surface of the MH electrode to form water. In a sealed system, these gas recombination reactions must occur at sufficient rates to avoid pressure buildup. This condition requires adequate electrode area, a thin electrolyte film, and, for the hydrogen absorption process, catalytic activity at the MH electrode surface to promote rapid dissociation of hydrogen.

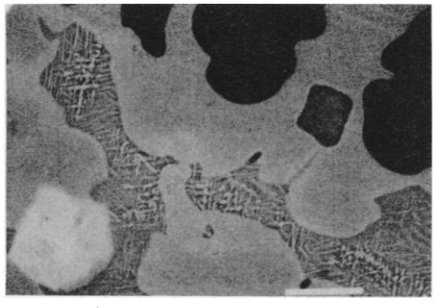

Fig. 1. Scanning electron micrograph of a bulk region of an Ovonic MH battery electrode that shows compositionally and structurally disordered multiphase alloy regions. Scale bar, 10 μm.

Chemical and Structural Disorder in Engineered Materials

The diverse properties required for a superior MH battery electrode can be attained by the engineering of new hydrogen storage materials on the basis of the concepts of structural and compositional disorder (*2*, *10–13*). Compositional and structural disorder is designed into the new MH materials on three different length scales through the use of elemental composition and processing techniques of alloys and electrodes. The length scales over which disorder is created can be designated: local (or atomic), which comprises regions with dimensions up to a few nearest-neighbor atomic distances; intermediate range, which comprises regions typically about 10 to 20 nm and extending up to about 100 nm; and long range, which involves regions with a dimension larger than about 100 nm. Disorder on each of these length scales is used to achieve different goals in the engineered alloys.

This approach allows one to consider a range of alloys for electrode materials containing elements that, if used alone, would be unacceptable for thermodynamic reasons, in particular oxidation or corrosion. Among the elements that become available for alloy formation in disordered electrode materials are Li, C, Mg, Al, Si, Ca, Ti, V, Cr, Mn, Fe, Co, Ni, Cu, Y, Zr, Nb, Mo, Sn, La, W, and Re. The list contains elements that can increase the number of hydrogen atoms stored per metal atom (Mg, Ti, V, Zr, Nb, and La). Other elements allow the adjustment of the metal-hydrogen bond strength (V, Mn, and Zr); provide catalytic properties to ensure sufficient charge and discharge reaction rates and gas recombination (Al, Mn, Co, Fe, and Ni); or impart desirable surface properties such as oxidation and corrosion resistance, improved porosity, and electronic and ionic conductivities (Cr, Mo, and W). The wide range of physical and chemical properties that can be produced in these alloys allows the MH battery performance to be optimized.

Compositional and structural disorder on a long-range length scale is used in the bulk of Ovonic MH alloys to give considerably higher hydrogen storage and better kinetics than possible in the conventional MH alloy structures, which are compositionally ordered and crystalline. The processing of disordered alloys can be optimized to produce polycrystalline, compositionally multiphase material. Figure 1 shows a scanning electron micrograph of a representative bulk region of a typical V, Ti, Zr, Ni, and Cr Ovonic MH alloy. Electron backscattering imaging was used to produce visual contrast between regions of the alloy that have different elemental compositions. This material contains five major distinct compositional phases as determined by energy-dispersive x-ray analysis. In addition, it has been determined separately by x-ray diffraction that the alloy contains three crystal structures: body-centered-cubic (bcc), hexagonal, and ^{14}C Laves crystal structures. From synthesis and characterization of separate, individual phases of a particular alloy, we conclude that the bcc structure can react to store large quantities of hydrogen (2.5% by weight) but lacks sufficient catalytic activity to be discharged at the required rates for battery applications. On the other hand, surrounding phases that may store less hydrogen but exhibit greater catalytic activity can effectively "channel" the hydrogen for rapid electrochemical discharge (*12*).

Intermediate-range structural and chemical disorder plays a number of important roles, primarily at interfaces both within the bulk of the MH electrode and at the electrode-electrolyte interface. Formation of the polycrystalline, compositionally multiphase bulk alloy gives rise to a high density of grain boundaries between com-

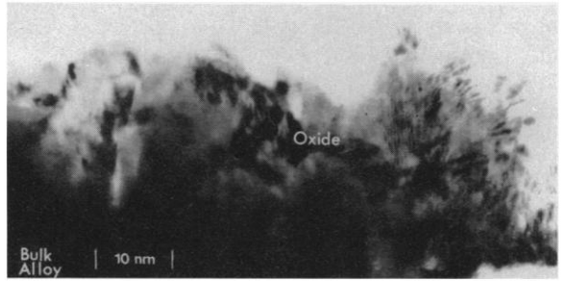

Fig. 2. Scanning transmission electron micrograph of the metal-electrolyte interface of an Ovonic MH battery electrode that shows the structure of the engineered multiphase bulk alloy and surface oxide.

positional and structural phases (for example, Fig. 1). The intermediate-range disorder that occurs at the grain boundaries increases surface area, which can greatly increase the density of catalytic sites. At the electrode-electrolyte interface, disorder on a length scale of approximately 10 to 100 nm is created during electrode processing and activation by the exploitation of chemical properties that are traceable to the elemental constituents of the MH alloy. The high-magnification scanning transmission electron micrograph of the electrode-electrolyte interface in Fig. 2 shows the presence of disorder on all three length scales but is particularly useful in illustrating the intermediate-range structural and compositional disorder that occurs in the engineered oxide layer that forms on the Ovonic MH electrode.

The basic Ovonic MH electrode typically contains elements such as V, Ti, Zr, Ni, and Cr. Although the alloy is a system with many characteristics such as MH bond strength that depend on interactions among the elemental constituents, some alloy properties are influenced by the chemistry of individual components. The primary role of V, Ti, and Zr in the alloy is hydrogen storage. All three elements, rather than just the least expensive (Ti), are used in the alloy for several reasons. Titanium and Zr form thick, dense, passive oxides in alkaline solutions, whereas V forms soluble oxides. These chemical characteristics are used in the preparation of the Ovonic MH electrode during the electrochemical activation step in which soluble oxides are intentionally corroded to produce intermediate-range structural disorder. This change gives rise to increased electrode surface area and microporosity and thereby increases charge acceptance. Chromium is used to limit the unrestrained corrosion of V and to control the alloy microstructure.

Zirconium contributes the important property of controlled hydrogen embrittlement, which leads to high surface area and, hence, to fast cell reactions. However, because excessive embrittlement can produce mechanical disintegration of the electrode that leads to poor electrical conductivity, high polarization, and low charge-recharge cycle life, one must control this property carefully in designing the electrode alloy.

Nickel serves several functions in the alloy. First, NiH has a weak bond strength. The bond strengths of elemental Ti, Zr, and V with hydrogen are too high for electrochemical applications. However, formation of alloys from these elements in various concentrations with Ni allows control of the alloy bond strength as was discussed earlier. Second, Ni is a catalyst for dissociation of H_2 and subsequent absorption of atomic H into the alloy. Third, Ni is resistant to oxidation. The combination of Ni with Zr, V, and Ti makes the alloy more resistant to oxidation and produces oxide films at the electrode-electrolyte interface that contain regions of metallic Ni. These regions help provide the necessary electrical conductivity and catalytic activity in the oxide film. The interface is characterized by a heterogeneous oxide region (Fig. 2) rather than a sharply defined homogeneous oxide film. We believe that this disordered oxide region is microporous and contains electrically conductive Ni regions that can catalyze the electrochemical discharge reaction (*14*).

Compositional disorder on the atomic scale is used to increase hydrogen storage capacity and improve catalytic activity through the incorporation into the MH alloy of elements that generate new chemically active sites. These sites offer an increased variety of hydrogen bonding possibilities and enhanced rates as a result of increased catalysis. Incorporation of elements with multidirectional *d* orbitals increases the range of stereochemical possibilities for bonding hydrogen, as confirmed by the increased amount of hydrogen absorbed and by increased catalytic activity. These effects also occur to a lesser extent with elements containing *f* orbitals that extend in still more directions than *d* orbitals but that are closer to the nucleus of the metal atom and, therefore, are less accessible.

Local compositional disorder is also used to adjust the metal-hydrogen bond strength in the MH alloy. Measurements of equilibrium hydrogen pressure versus MH hydrogen concentration at 30°C are shown in Fig. 3 for a series of multicomponent MH alloys in which the ratio of V to Zr is systematically varied. The equilibrium hydrogen pressure, p, in these measurements is related to the change in Gibbs free energy, ΔG, which occurs for the reaction between gaseous hydrogen and the hydrogen storage alloy to form MH. This value can be written:

$$\Delta G = \Delta H - T\Delta S = RT \ln p \qquad (3)$$

Because the entropy term, $T\Delta S$, is small at room temperature compared with the enthalpy change, ΔH largely determines ΔG. Thus, determination of p provides a measure of ΔH, which is related to the metal-hydrogen bond strength. In Fig. 3, variations in the ratio of V to Zr give rise to the observed changes in p for a given hydrogen concentration in the MH alloy. This result indicates that these compositional variations have changed the metal-hydrogen bond strength.

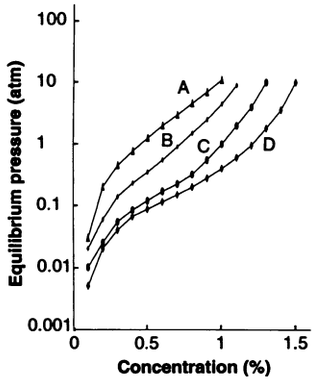

Fig. 3. Equilibrium hydrogen pressure versus hydrogen concentration (percent by weight) at 30°C for a series of Ovonic MH electrode alloys. Data show how variation in alloy composition may be used to control metal-hydrogen bond strength. The MH alloy compositions shown here, expressed as atomic percent, are (**A**) ($V_{21}Ti_{15}Zr_{15}Ni_{31}Cr_6Co_6Fe_6$), (**B**) ($V_{15}Ti_{15}Zr_{21}Ni_{31}Cr_6Co_6Fe_6$), (**C**) ($V_{18}Ti_{15}Zr_{18}Ni_{31}Cr_6Co_6Fe_6$), and (**D**) ($V_{15}Ti_{15}Zr_{20}Ni_{28}Cr_5Co_5Fe_6Mn_6$).

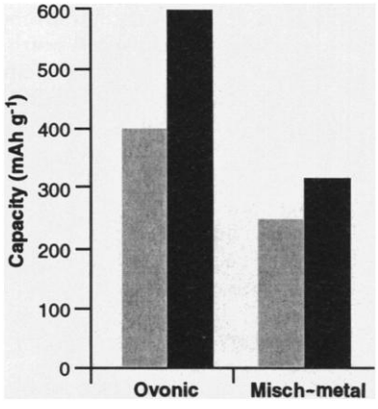

Fig. 4. Comparison of the charge storage capacity of present (shaded bars) and projected (solid bars) Ovonic MH battery and misch-metal ($LaNi_5$) electrodes.

Status of the Ovonic Battery

The storage capacity of current and future Ovonic MH electrodes is shown in Fig. 4, along with the storage capacity of current and improved conventional $LaNi_5$, or "misch-metal," MH electrodes. The latter materials are frequently referred to as misch metal because they are traditionally made from a mixture of naturally occurring rare-earth elements that can include Ce, La, Nd, and Pr. The data for current electrodes were obtained from electrochemical half-cell measurements of commercial Ovonic and misch-metal battery electrodes, as described in (*11*). Data for projected misch-metal electrodes are from (*15*) and are based on electrochemical half-cell measurements of prototype materials. Data for projected Ovonic MH electrodes are based on electrochemical measurements of advanced laboratory thin-film materials.

The USABC contract contains three main program goals: a scale-up from small portable cells (1 to 5 Ah) to large EV cells (50 to 250 Ah), an increase in energy density from 56 to 80 Wh kg^{-1}, and the construction of series-connected battery modules to produce the voltages required for EV propulsion (180 to 320 V). The performance capabilities of the present Ovonic NiMH technology are shown in the second column of Table 1. To a large extent, prototype batteries of several designs and sizes have demonstrated performance characteristics that satisfy or exceed individual USABC midterm goals shown in the first column. Efforts to optimize all performance characteristics within a particular cell design are an ongoing activity. Another program objective, scale-up of cell size, has also been achieved. The ability to manufacture batteries with this technology has been demonstrated by OBC and several of its licensees who have been producing small portable batteries since 1987. Series-connected battery modules up to 40 V have been constructed by OBC and are under test. A 12-V, 3-kWh module is shown in Fig. 5.

Comparison with Other Candidates for EV Batteries

Battery characteristics have a dominant influence on overall EV performance. For example, battery-specific energy (in watt-hours per kilogram) controls vehicle range. Similarly, battery power (in watts per kilogram) translates into vehicle acceleration. The Bertone Blitz, a high-performance prototype EV sports car (*16*), has achieved an impressive acceleration of 0 to 100 km per hour (0 to 62 miles per hour) in 6 s, in part through the use of Ni-Cd batteries with high peak power. Some candidate battery technologies for EV applications are listed in Fig. 6, which shows a comparison plot of peak power versus depth of discharge. These measurements were made independently at Argonne National Laboratories (*17*). High peak power (>150 W kg^{-1}), as required by the USABC goals shown in Table 1, must be maintained over the entire depth of discharge of the battery for satisfactory vehicle performance. The Ovonic NiMH battery provides the highest peak power and can maintain it over almost the full range of discharge.

Although Ni-Cd is a rechargeable battery technology with high peak power that is extensively used in consumer products such as electronic devices and power tools, its energy density does not meet USABC requirements, it uses toxic materials (Cd), and in the large sizes used for EVs, it is not a totally sealed system.

The Na-S battery has a high energy density, but its low peak power is a significant deficiency. In addition, the operating temperature of the battery is approximately 300°C, which must be maintained at all times because the battery can withstand only a few cycles of cooling and heating. The presence of molten sodium and sulfur is potentially hazardous, and corrosion has limited the reliability and life of prototype batteries.

Of the remaining batteries shown in Fig. 6, only the Pb-acid battery has been tested sufficiently to serve as a practical, immediate candidate for EV applications. However, its typical energy density of 30 Wh kg^{-1} is substantially below USABC requirements, and its limited cycle life would force it to be replaced every 32,000 km (20,000 miles).

Long cycle life is a feature of the Ovonic NiMH battery technology that will have economic consequences for EVs. Over 1000 charge-discharge cycles at 100% depth of discharge have been demonstrated (*13*) with Ovonic batteries. Under conditions of 30% depth of discharge, Ovonic NiMH cells designed for aerospace applications have demonstrated (*18*) a lifetime of more than 10,000 cycles. It is expected that in EV applications, batteries will experience a typical depth of discharge of about 80%. Under these conditions the cycle life of the Ovonic NiMH battery is projected to be 2000 to 3000 cycles, according to a numerical model (*18*).

Battery cycle life can be converted into EV battery-life driving range when the characteristics of the EV are specified. For example, in a GM Impact-type vehicle, replacement of the Pb-acid battery with an Ovonic NiMH system of the same volume increases its range to 480 km (300 miles). For 80% depth of discharge [385 km (240 miles)], even a conservative estimate of 500 cycles for the battery life will give a 200,000-km (120,000-mile) battery-life driving range. The electrical energy necessary to provide the 385-km range per charge costs only $2.32 at $0.08 per kilowatt-hour, compared with approximately $14 worth of gasoline needed to provide the same range for a typical IC-powered vehicle. Lifetime EV maintenance costs will also be smaller than for typical IC-powered vehicles. Therefore, EVs that are powered by batteries with long cycle lives and that meet the USABC initial cost goal of $150 per kilowatt-hour can be economically competitive on a lifetime basis.

Technology Improvements

The range of an EV will depend on many factors besides battery energy density, such as vehicle weight, tire rolling friction, and electric motor efficiency. Information published by GM on its pioneering Impact vehicle can be used to establish a benchmark for conversion of battery energy density to vehicle range (*19*) for EVs of this type. The data from GM show that their vehicle will travel 180 km (113 miles) with a battery that stores 13.5 kWh. For a battery of the same weight, the current Ovonic NiMH technology will, therefore,

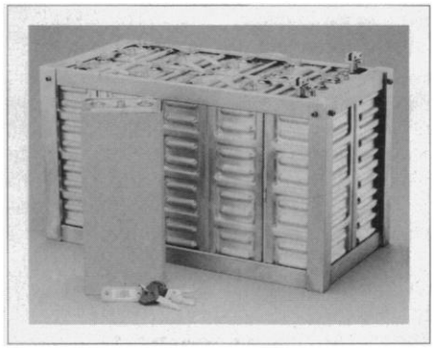

Fig. 5. A 3-kWh, 12-V series-connected Ovonic NiMH battery module and 250-Ah Ovonic NiMH single cell.

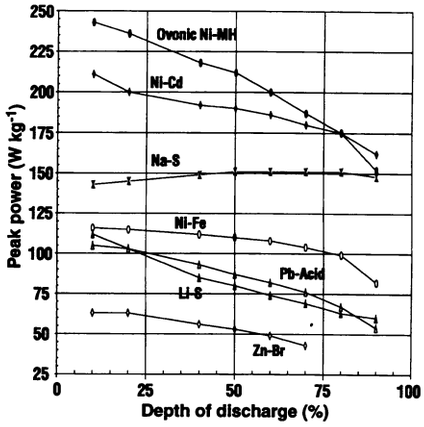

Fig. 6. Peak power versus depth of discharge, as measured (*17*) at Argonne National Laboratories, for a number of candidate EV battery technologies.

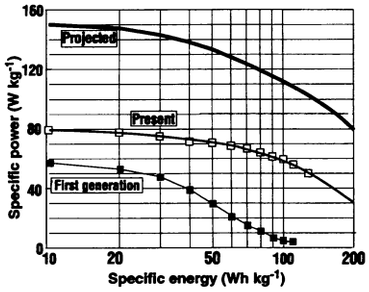

Fig. 7. Specific energy versus specific power for first-generation, present, and projected Ovonic NiMH batteries. Data shown for first-generation devices were obtained from 4-Ah "C" size cells; data for present devices were obtained from 50-Ah prismatic cells.

provide 31.6 kWh of energy storage, which will provide a vehicle range of 415 km (264 miles). For the same battery volume, the Ovonic NiMH battery will increase the range per charge to 480 km (300 miles). The environmental impact of eventual disposal of the Ovonic NiMH battery has also been studied (*20*). Knoll and colleagues concluded that, according to existing Environmental Protection Agency regulations, batteries that use this technology can be safely disposed of in landfills. It has also been shown (*21*) that with existing technology, Ovonic batteries can be recycled into metallurgical additives for cast iron, stainless steel, or new Ovonic NiMH battery electrodes. The commercial viability of each of these technologically feasible recycling programs will depend on process economics.

Future developments of Ovonic NiMH batteries will include improvements through the continued optimization of the MH materials and electrodes as well as improvements to the positive electrode and cell design (*2*). For example, some of the ongoing research at OBC focuses on application of the company's synthetic materials techniques to the development of an improved positive electrode with enhanced storage capacity through the use of engineered valence control. The chemical reaction that occurs during the charge of a conventional $Ni(OH)_2$ electrode involves transfer of one electron per Ni atom. We are developing materials that use the exchange of up to two electrons per atom. In addition, MH alloys with twice the storage capacity of first-generation materials have been measured in the laboratory, and cell designs in which lightweight substrates, current collection components, and containers are used are now being developed. Because the overall energy density of the battery is determined by the entire system, these combined approaches are targeted at the fabrication of batteries with both an energy storage density of 150 Wh kg^{-1} and the characteristics shown in Fig. 7.

Conclusion

In the development of the Ovonic NiMH battery, we have used aspects of physics, chemistry, metallurgy, and materials science. In particular, materials concepts (*10–13*) were focused on structural and compositional disorder to develop an NiMH battery with the characteristics necessary for practical EV use in the near, middle, and distant future.

REFERENCES AND NOTES

1. P. Jaret, *EPRI J.* **4**, 4 (1992).
2. S. R. Ovshinsky and M. A. Fetcenko, U.S. Patent 5 135 589 (1992); 23 additional patents.
3. M. A. Gutjahr, H. Buchner, K. D. Beccu, H. Saufferer, in *Power Sources 4*, D. H. Collins, Ed. (Oriel, Newcastle upon Tyne, United Kingdom, 1973), p. 79.
4. A. Percheron-Guegen, U.S. Patent 4 107 405 (1978).
5. M. H. J. van Rijswick, in *Proceedings of the International Symposium on Hydrides for Energy Storage* (Pergamon, Oxford, 1978), p. 261.
6. G. Halpert, in *Proceedings of the Symposium on Nickel Hydroxide Electrodes*, Electrochemical Society, Hollywood, FL, 16 to 18 October 1989 (Electrochemical Society, Pennington, NJ, 1990), pp. 3–17.
7. E. J. McHenry, *Electrochem. Technol.* **5**, 275 (1967).
8. T. A. Edison, U.S. Patent 1 402 751 (1922).
9. S. U. Falk and A. J. Salkind, *Alkaline Storage Batteries* (Wiley, New York, 1969).
10. S. R. Ovshinsky, *J. Non-Cryst. Solids* **32**, 17 (1979); for additional references, see S. R. Ovshinsky, *Disordered Materials: Science and Technology—Selected Papers*, D. Adler, B. B. Schwartz, M. Silver, Eds. (Institute for Amorphous Studies Series, Plenum, New York, ed. 2, 1991).
11. K. Sapru, B. Reichman, A. Reger, S. R. Ovshinsky, U.S. Patent 4 623 597 (1986).
12. M. A. Fetcenko, S. Venkatesan, K. C. Hong, B. Reichman, in *Proceedings of the 16th International Power Sources Symposium* (International Power Sources Committee, Surrey, United Kingdom, 1988), p. 411.
13. S. R. Ovshinsky, S. Venkatesan, M. Fetcenko, S. Dhar, in *Proceedings of the 24th International Symposium on Automotive Technology and Automation* (Automotive Automation, Croyden, United Kingdom, 1991), p. 29.
14. M. A. Fetcenko, S. Venkatesan, S. R. Ovshinsky, in *Proceedings of the Symposium on Hydrogen Storage Materials, Batteries, and Electrochemistry* (Electrochemical Society, Pennington, NJ, 1992), p. 141.
15. M. Tadokoro, K. Moriwaki, M. Nogami, T. Ise, N. Furakawa, in *ibid.*, p. 92.
16. L. Ciferri, *Autoweek* **1992**, 14 (7 September 1992).
17. W. H. DeLuca, paper presented at the 1991 Annual Automotive Technology Development Contractors Coordination Meeting, Dearborn, MI, 24 October 1991.
18. B. Otzinger, in *Proceedings of the 6th Annual Battery Conference on Applications and Advances* (California State University, Long Beach, 1991).
19. *General Motors Electric Vehicles Progress Report* (summer 1992).
20. C. R. Knoll, S. M. Tuominen, J. R. Peterson, T. R. McQueary, in *Proceedings of Battery Waste Management Seminar*, S. Wolsky, Ed. (Ansum Enterprises, Deerfield Beach, FL, 1990).
21. C. R. Knoll, S. M. Tuominen, R. E. Walsh, J. R. Peterson, in *Proceedings of the 4th International Seminar on Battery Waste Management*, S. Wolsky, Ed. (Ansum Enterprises, Deerfield Beach, FL, 1991).

22. We thank the research staff at Energy Conversion Devices–OBC, particularly S. Venkatesan, for their contributions to the developments described in this article and S. J. Hudgens for his critical comments and helpful suggestions during preparation of the manuscript.

RESEARCH ARTICLES

Regulation of Gene Expression in Hippocampal Neurons by Distinct Calcium Signaling Pathways

Hilmar Bading,* David D. Ginty, Michael E. Greenberg†

Calcium ions (Ca^{2+}) act as an intracellular second messenger and can enter neurons through various ion channels. Influx of Ca^{2+} through distinct types of Ca^{2+} channels may differentially activate biochemical processes. *N*-Methyl-D-aspartate (NMDA) receptors and L-type Ca^{2+} channels, two major sites of Ca^{2+} entry into hippocampal neurons, were found to transmit signals to the nucleus and regulated gene transcription through two distinct Ca^{2+} signaling pathways. Activation of the multifunctional Ca^{2+}-calmodulin–dependent protein kinase (CaM kinase) was evoked by stimulation of either NMDA receptors or L-type Ca^{2+} channels; however, activation of CaM kinase appeared to be critical only for propagating the L-type Ca^{2+} channel signal to the nucleus. Also, the NMDA receptor and L-type Ca^{2+} channel pathways activated transcription by means of different cis-acting regulatory elements in the c-*fos* promoter. These results indicate that Ca^{2+}, depending on its mode of entry into neurons, can activate two distinct signaling pathways. Differential signal processing may provide a mechanism by which Ca^{2+} controls diverse cellular functions.

In neurons, transient changes in the concentration of intracellular calcium ($[Ca^{2+}]_i$) can trigger various processes including neurotransmitter release, modulation of synaptic transmission, excitotoxic cell death, and alterations in gene expression (*1*, *2*). The concentration of intracellular Ca^{2+} can be increased by Ca^{2+} influx across the plasma membrane and by release of Ca^{2+} from internal stores (*3*). To control Ca^{2+} entry, neurons have multiple types of Ca^{2+}-permeable ion channels (*4*). The segregation of Ca^{2+} channels into distinct subcellular regions of neurons may serve to generate highly localized Ca^{2+} signals (*5*). Consequently, the mode of Ca^{2+} entry into neu-